CSIRO Publishing

Publications of the Astronomical Society of Australia

VOLUME 19, 2002

An international journal of astronomy and astrophysics

For editorial enquiries and manuscripts, please contact:
The Editor, PASA,
ATNF, CSIRO,
PO Box 76,
Epping, NSW 1710, Australia
Telephone: +61 2 9372 4590
Fax: +61 2 9372 4310
Email: Michelle.Storey@atnf.csiro.au

For general enquiries and subscriptions, please contact:
CSIRO Publishing
PO Box 1139 (150 Oxford St)
Collingwood, Vic. 3066, Australia
Telephone: +61 3 9662 7666
Fax: +61 3 9662 7555
Email: publishing.pasa@csiro.au

Published by CSIRO Publishing
for the Astronomical Society of Australia

www.publish.csiro.au/journals/pasa

Publ. Astron. Soc. Aust., 2002, 19, 505–514

A Spectral Line Survey of IRAS 17470-2853 from 86.1 to 92.1 GHz

Hun-Dae Kim[1], Ramesh Balasubramanyam[1] and Michael G. Burton[1,2]

[1]School of Physics, University of New South Wales, Sydney, NSW 2052, Australia
[2]School of Cosmic Physics, Dublin Institute for Advanced Studies, 5 Merrion Square, Dublin 2, Ireland

Received 2001 September 15, accepted 2002 October 6

Abstract: We present results from a spectral line survey of the young stellar object IRAS 17470-2853, undertaken to examine chemical changes during the evolution from hot molecular cores to ultracompact HII regions. Observations were carried out with the Mopra 22 m radio telescope in the frequency range from 86.1 to 92.1 GHz. A total of 21 lines from 9 molecules were detected. Except for CH_3CN they are all simple molecules. We compare the results to the ultracompact HII region G34.3+0.15, where spectral line surveys in the frequency range 80–115 GHz and 330–360 GHz have been performed. While the molecular lines detected are similar, their widths and intensities are somewhat narrower and lower, respectively, in IRAS 17470-2853. The typical line width of $\sim$5 km s^{-1} indicates relatively quiet or quasi-thermal emission. On the other hand, a significant difference in T_A^*(HNC)/T_A^*(HCN) has been found: 0.8 for IRAS 17470-2853 compared to 2.6 for G34.3+0.15. The broad line width of SiO ($v = 0$, $J = 2$–1), $\sim$9 km s^{-1}, suggests that IRAS 17470-2853 is experiencing a shock generated by the embedded object. Column densities, or lower limits to them, are derived for observed molecules.

Keywords: HII regions — ISM: individual (IRAS 17470-2853 = G0.55–0.85) — ISM: molecules — ISM: abundances — stars: formation — radio lines: ISM

1 Introduction

Understanding the relation between the stage that star formation has reached and the chemical state of a molecular cloud has long been of interest, since young stellar objects (YSOs) drive the chemical evolution of molecular clouds, especially adjacent to a hot core. A hot core is characterised by small volume, high density, and warm temperature (typically $R \sim 0.01$–0.1 pc, $n \sim 10^6$–10^8 cm^{-3}, $T \sim 100$–300 K: Henkel et al. 1987; Walmsley et al. 1987), and is associated with an embedded protostar. Hot cores are also distinguished from cold cores through their high abundance of saturated molecules such as CH_3OH, NH_3, CH_3CN, CH_3CH_2OH, and H_2CS. The high abundance of such complex molecules cannot be explained solely by pure gas phase reactions in the cloud, but requires grain surface chemistry. Even though the details of how the chemistry works remain controversial, the models (e.g., Millar, Herbst, & Charnley 1991; Charnley et al. 1995) produce reasonably close agreement with observational results. In grain surface models the high abundance of complex molecules is due to hydrogenation and nitrogenation of atoms and molecules that are deposited onto the dust mantles as the molecular clouds undergo gravitational collapse. As star formation commences, radiation from the embedded protostar evaporates the molecules from the dust mantles. Accordingly, star formation determines the overall chemical reactions and evolution of the parent molecular clouds.

Through an understanding of these chemical properties we can trace the evolutionary phase of molecular clouds by comparing chemical models to observation. Star-forming clouds for which chemical models have been developed include Orion–KL (Charnley et al. 1995) and G34.3+0.15 (Millar, Macdonald, & Gibb 1997). The models are reasonably successful, but they require the inclusion of more complicated reaction routes, detailed calculations of collision rates, and improvements to their time-dependent behaviour to provide a more precise explanation for the observational data. Molecules such as CH_3CN, CH_3OH, and NH_3, believed to probe the hot cores, have been widely used to delineate their chemical properties. However, they are not enough to derive the overall state of star-forming molecular clouds, which comprise a range of temperatures and densities from cold gas to hot cores. Changes occurring within the hot core then influence the chemistry within the ambient molecular cloud, through both the radiation field and outflows that are generated. Hence, a study of both the cold gas and hot core region of clouds is required to provide a more comprehensive understanding of the effects of star formation on and in molecular clouds.

Molecular line surveys satisfy these requirements. Their wide frequency range includes emission from many species and their transitions have a wide range of excitation energy. Comparison of detected molecules and their transitions between sources allows us to examine the variation in chemical properties from source to source. If many transitions from a molecule are detected, it is possible to estimate excitation temperatures and molecular abundances by means of the rotation diagram method (e.g., see Macdonald et al. 1996). While extensive observations have been carried out on the sources Orion–KL (e.g., Johansson et al. 1984; Jewell et al. 1989; Turner 1989; Blake et al. 1986, 1996; Ziurys & McGonagle 1993; Schilke et al. 1997) and Sgr B2 (e.g., Cumins, Linke, & Thaddeus 1986; Turner 1989; Sutton et al. 1991), a wider range of sources is needed in order to investigate

 10.1071/AS01094 1323-3580/02/04505$05.00

the chemical evolution underway. Therefore, we undertook a molecular line survey of the young stellar source IRAS 17470-2853 to examine its physical and chemical properties. We have compared these to the ultracompact HII region G34.3+0.15, because G34.3+0.15 seems to be more alike in evolutionary stage and physical properties than Orion–KL or Sgr B2 are.

Walsh et al. (1997, 1998) undertook a survey of ultracompact HII regions for emission from the 6.669 GHz methanol maser, to examine the association between these two signposts of star formation. Among their sources IRAS 17470-2853 (also known as G0.55–0.85) was included. Its distance is inferred to be 2 kpc and the radial velocity range of the methanol masers is +8 to +19 km s^{-1}. Also measured from this source is radio and sub-mm continuum emission, OH and water maser emission (see Walsh et al. 1998, 1998, 2002; Forster & Caswell 1999). The OH masers have similar velocity range to the methanol masers (+8 to +20 km s^{-1}), but the water masers are spread over a larger velocity range, from −13 to +57 km s^{-1}. The radio and sub-mm continuum emission consists of a bright core, embedded in diffuse emission extending mostly NW–SE of it. The methanol and OH maser sites also are coincident with the continuum core, and the OH maser sites appear to extend somewhat in a direction NW–SE. The water maser sites are located ∼2″ NW of the OH and CH_3OH masers. The source also appears in the MSX[1] survey at mid-infrared wavelengths, as one of six sources embedded in diffuse emission over a 30′ region. It is also visible as a faint red source in the 2MASS near-infrared survey, with a [1.65 μm] – [2.2 μm] colour of 2.4 magnitudes. The bolometric luminosity of the source has been estimated as $\sim 1.3 \times 10^4$ $L_\odot$ (Walsh et al. 2002), the equivalent of a B0.5 main sequence star. For reference, the fluxes from near-infrared to radio wavelengths are tabulated in Table 1. To aid identification of the features, Figure 1, adapted from Walsh et al. (2002), shows the sub-mm continuum emission, and the positions of the methanol masers, radio continuum emission, and sources from the MSX point source catalogue.

From their survey Walsh et al. (1998) concluded that methanol maser emission arises before the onset of ultracompact HII region formation, and disappears sometime after its expansion towards an HII region. The detection of methanol maser emission with relatively weak radio continuum from IRAS 17470-2853 suggests that it is probably less evolved than G34.3+0.15. Accordingly, our investigation with the Mopra telescope sought to examine whether the chemical state of the source supported this supposition that it is in an earlier evolutionary stage.

2 Observations

Observations of IRAS 17470-2853 in the frequency range 86.1–92.1 GHz were made using the Mopra 22 m radio telescope between 20 and 30 November 2000. The position observed was $17^h50^m14.5^s$, −28°54′31.2″ (J2000), with a sky position $+1^m$ away in longitude. The beam size is 40″ and the forward spillover and scattering efficiency ($\eta_{\rm fss}$) of the telescope is 0.6. The receiver employed was a dual polarisation, low noise SiS mixer, with an autocorrelator configured to have 512 channels of 500 kHz width each (∼1.5 km s^{-1}). This allowed 256 MHz coverage for each local oscillator (LO) setting. In the course of

[1]For MSX and 2MASS infrared survey archives see http://irsa.ipac.caltech.edu.

Table 1. Continuum fluxes of IRAS 17470-2853 (G0.55–0.85)

Wavelength (μm)	Flux (Jy)
1.25[1]	2.0 (−4)
1.65[1]	1.2 (−3)
2.2[1]	6.8 (−3)
8.3[2]	1.6 (+1)
12.1[2]	2.7 (+1)
14.6[2]	3.3 (+1)
21.3[2]	1.4 (+2)
450[3]	4.4 (+2)
850[3]	4.7 (+1)
34 700[4,5]	7.0 (−2)

In the Flux column $2.0(-4) \equiv 2.0 \times 10^{-4}$, etc.
[1] From 2MASS archive for source at $17^h50^m14.4^s$, −28°54′26″ (J2000); [2] From MSX archive for source at $17^h50^m14.4^s$, −28°54′28″ (J2000); [3] From Walsh et al. (2002) for source at $17^h50^m14.2^s$, −28°54′30″ (J2000); [4] From Walsh et al. (1998) for source at $17^h50^m14.5^s$, −28°54′30″ (J2000); [5] More usually written as 8.64 GHz.

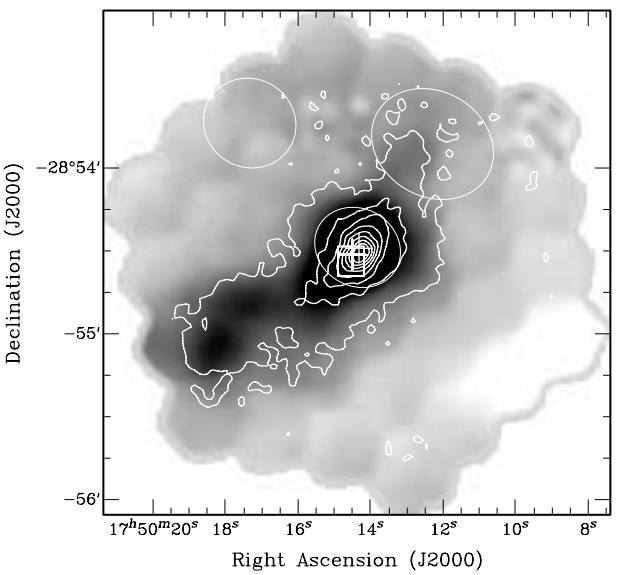

Figure 1 Image of the 850 μm emission from IRAS 17470-2853, overlaid with contours of the 450 μm emission (adapted from Walsh et al. 2002). Also shown with crosses are the positions of methanol maser sites, with a square the position of the radio continuum emission from an ultracompact HII region, and with ellipses the positions of MSX sources from the Point Source Catalogue (version 1.2).

observations the typical system temperature ranged from 200 to 400 K. Observations were carried out in position-switched mode, with 30 s on-source and 30 s off-source, repeating typically 20 times. The same LO frequency was set for both polarisation A and B, improving the RMS noise by a factor of $\sqrt{2}$. The system provides a theoretical RMS noise of 0.03–0.04 K, allowing the identification of lines with antenna temperature T_A^* of $\sim$0.1 K (3σ). Pointing was checked every 2–3 h, targeting an SiO 86 GHz maser point source, VX–Sgr.

With some considerable tuning and pointing overheads, we obtained 3–4 spectra of 256 MHz bandwidth during each 6 h observing session. Flux calibration was done with standard chopper wheel method (Ulich & Haas 1976), giving the intensity on the antenna temperature scale, T_A^*.

3 Spectral Reduction and Line Identification

Reduction of the spectral scans was undertaken with the AIPS++ DISH tool (Garwood & McMullin 1999), together with custom-written auxiliary programs. In averaging spectra from individual scans, those with poor baselines were first discarded, a 3rd order polynomial fit to the continuum and the baseline then subtracted off. The typical RMS noise achieved per spectrum was 0.05 K, about a factor 2 worse than theoretically possible if no bad scans were thrown out. The signal at the edge of the bandpass was usually poor and so discarded, leading to some small gaps in spectral coverage. The spectra from each resulting $\sim$200 MHz band were then combined with neighbouring bands, so each panel presented in Figure 2 covers about 800 MHz. For line identification, we used the Lovas catalogue (Lovas 1992) exclusively, because the frequency 86–92 GHz has been fully covered in other line surveys.

Central frequencies for each line stronger than 3σ were determined through Gaussian fitting, after correcting for the Doppler shift of $+14\,\mathrm{km\,s^{-1}}$. A total of 21 lines, including blended lines, from 9 species were detected (see Table 2). All the lines have also been detected in G34.3+0.15 (Kim et al. 2000). There are also some notable differences, however, from G34.3+0.15, as discussed in Section 4. As anticipated, the spectrum is somewhat different from that of Orion–KL (Turner 1989), reflecting the different chemical state of the sources.

4 Individual Molecules

In Figure 3 we compare the measured values of T_A^*, FWHM, and intensity ($\int T_A^* dv$) for IRAS 17470-2853 with those for G34.3+0.15 obtained with the 14 m Taeduk Radio Astronomy Observatory (TRAO) telescope. This figure demonstrates graphically the difference in physical parameters derived for molecules in the two sources, although the different beam sizes render the Mopra results more sensitive to compact (i.e. unresolved) emission. In general the intensities, T_A^*, are similar, except for HCN which is four times brighter in IRAS 17470-2853. The typical line width in IRAS 17470-2853, $\sim$5 km s^{-1}, is somewhat narrower than G34.3+0.15. The SiO ($v=0$, $J=2$–1) line has a broader line width (9.1 km s^{-1}), although it is also slightly narrower than in G34.3+0.15 (where it is 10.0 km s^{-1} wide).

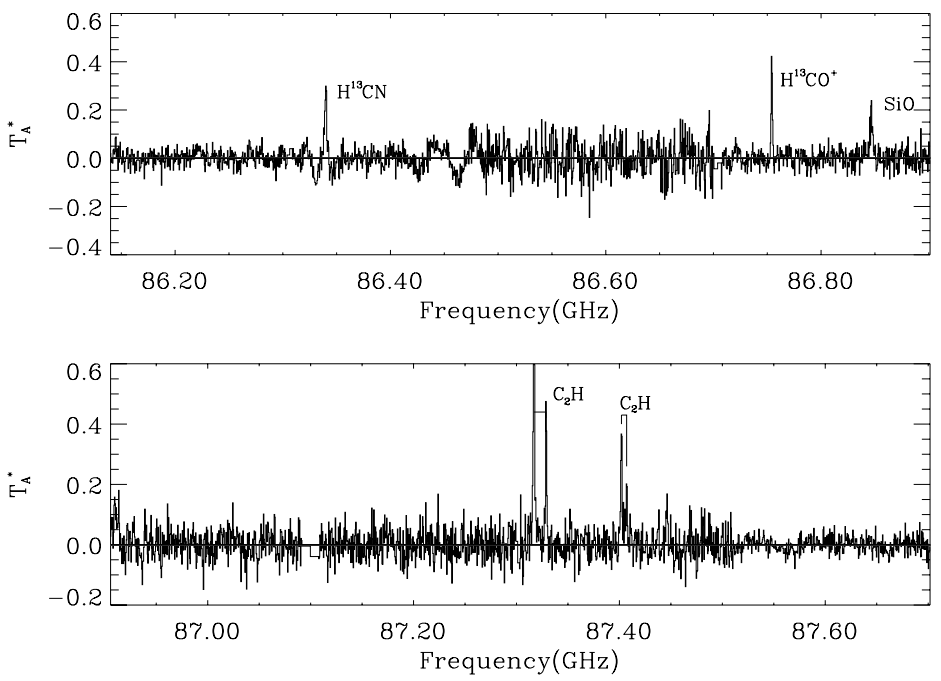

Figure 2 Spectra of the 86.1–92.1 GHz line emission from IRAS 17470-2853. Each panel is 800 MHz wide, combining four neighbouring frequency bands. Detected lines are labelled with their molecule. The intensity scale is T_A^* and the frequency scale is in GHz.

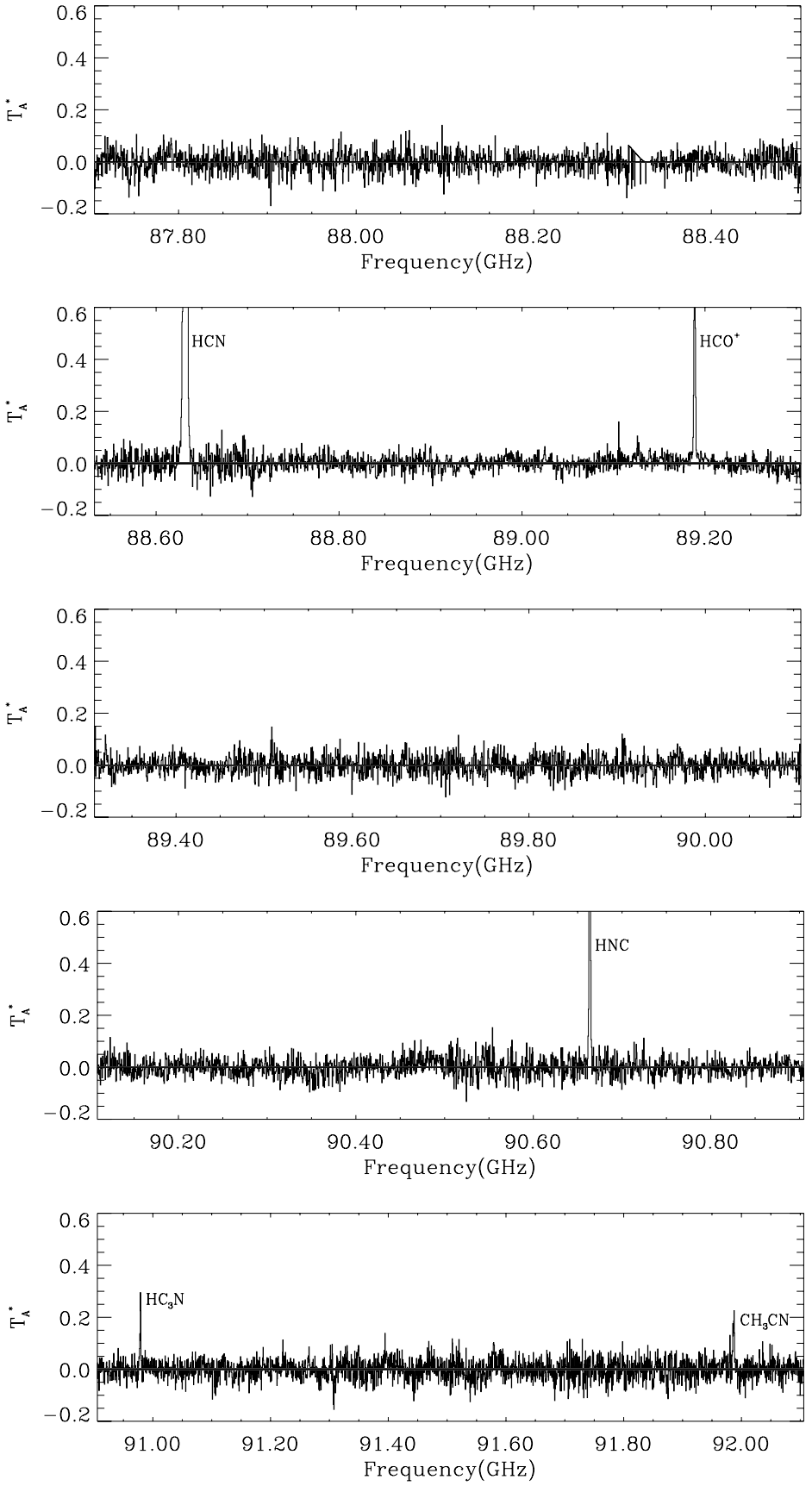

Figure 2 (*continued*)

Table 2. Observed molecular line parameters[a]

ν (obs)[b] (GHz)	T_A^* (K)	Δv (km s^{-1})	Species	Transition	ν (rest) (GHz)	$\int T_A^* dv^c$ (K km s^{-1})	Notes
86.3398	0.3*	8.6	$H^{13}CN$	1–0 $F=1$–1	86.3388	2.6	bld
			$H^{13}CN$	1–0 $F=2$–1	86.3402		bld
			$H^{13}CN$	1–0 $F=0$–1	86.3423		
86.7542	0.4	4.7	$H^{13}CO^+$	1–0	86.7543	2.2	
86.8467	0.2	9.1	SiO	2–1 $v=0$	86.8470	1.7	
87.3170	0.8	5.1	C_2H	1–0 3/2–1/2 $F=2$–1	87.3169	4.4	
87.3287	0.5	4.8	C_2H	1–0 3/2–1/2 $F=1$–0	87.3286	2.0	
87.4019	0.4	5.2	C_2H	1–0 1/2–1/2 $F=1$–1	87.4020	2.1	
87.4071	0.2	3.6	C_2H	1–0 1/2–1/2 $F=0$–1	87.4072	0.8	
87.4461	0.1	6.0	C_2H	1–0 1/2–1/2 $F=1$–0	87.4465	0.9	
88.6318	2.9*	15.9	HCN	1–0 $F=1$–1	88.6304	36.9	bld
			HCN	1–0 $F=2$–1	88.6318		bld
			HCN	1–0 $F=0$–1	88.6339		bld
89.1887	1.4	4.5	HCO^+	1–0	89.1885	6.5	
90.6635	2.4*	4.2	HNC	1–0 $F=0$–1	90.6635	11.7	bld
			HNC	1–0 $F=2$–1	90.6636		bld
			HNC	1–0 $F=1$–1	90.6637		bld
90.9790	0.3	5.8	HC_3N	10–9	90.9790	1.5	
91.9806	0.1	2.9	CH_3CN	$J=5$–4, $K=2$	91.9801	0.4	
91.9868	0.2*	10.5	CH_3CN	$J=5$–4, $K=1$	91.9853	2.1	bld
			CH_3CN	$J=5$–4, $K=0$	91.9871		bld

[a]Molecules and their transitions detected in the frequency range of 86.1–92.1 GHz. Blended lines are marked with 'bld' in the notes column. The flux listed is for the sum of all lines in the blend.
[b]Observed frequencies after correcting the Doppler shift with the velocity of the local standard of rest, +14 km s^{-1} (Walsh et al. 1997). The full-width half-maximum (FWHM) and antenna temperature (T_A^*) of each line are derived from Gaussian fitting, except for T_A^* for HNC and HCN, where the peak value of the signal is used.
[c]* in the T_A^* column refers to the peak value of the signal in blended lines.

4.1 HCO^+, HCN, and HNC

HCO^+, HCN, and HNC are all detected in IRAS 17470-2853. The isotopes $H^{13}CN$ and $H^{13}CO^+$ are also detected, and the relevant isotopic line ratios are HCN/$H^{13}CN$ ~ 9 and $HCO^+/H^{13}CO^+$ ~ 3.

HCO^+

Figure 4 compares the HCN and HCO^+ profiles in IRAS 17470-2853 and G34.3+0.15. No self-absorption feature is seen in the HCO^+ (1–0) line in IRAS 17470-2853, unlike in G34.3+0.15, where there is a dip in the profile at +3 km s^{-1}. This suggests that IRAS 17470-2853 is surrounded by a relatively thinner colder layer than G34.3+0.15, so the emission passes through the foreground cloud without absorption.

HCN

When optically thin, the ratio of the $F=1$–1, 2–1 and 0–1 hyperfine transitions of HCN is 3:5:1, i.e. the ratio of the level degeneracies. While the 2–1 and 0–1 lines are blended in our data, the observed ratio in IRAS 17470-2853 is clearly ∼3:5:3 rather than 3:5:1. These ratios are very different, however, to those measured in G34.3+0.15 (which are ∼6:5:2; see Figure 4), which we attribute to optical depth effects in the 2–1 and 1–1 lines in that source. For instance, Cernicharo et al. (1984) suggest that such anomalous ratios can arise due to the scattering of these two lines by a diffuse envelope surrounding an optically thick hotter core, while leaving the optically thin 0–1 line unattenuated.

HNC

The isomers HCN and HNC have a similar energy level structure and almost identical dipole moments: $\mu = 2.98$ debyes for HCN and 3.05 for HNC. They also have the same pre-cursor molecules, $HCNH^+$ and H_2CN^+ (Brown, Burden, & Cuno 1989). Therefore one expects a similar abundance ratio for the two isomers. However, the ratio $T_A^*(\mathrm{HNC})/T_A^*(\mathrm{HCN})$ is very different between the sources: 0.8 in IRAS 17470-2853 and 2.6 in G34.3+0.15. The higher ratio in G34.3+0.15 might arise from self-absorption in the HCN line, as discussed above. However, if self-absorption is not significant for the HCN line, then the difference in HNC/HCN ratios may mark a physical difference between the environment in the two sources (e.g., see Schilke et al. 1992), with a greater abundance of HNC in IRAS 17470-2853. If so, then measurement of this line ratio provides a tool to study the change of physical state in evolving hot molecular cores.

It would, however, be unusual to have a greater abundance of HNC than HCN. For instance, in a study of molecular abundances in 13 molecular clouds Wootten et al. (1978) found that in most sources the abundance ratio of HNC/HCN is less than 1. Baudry et al. (1980) also found in a study towards 9 molecular clouds that HNC

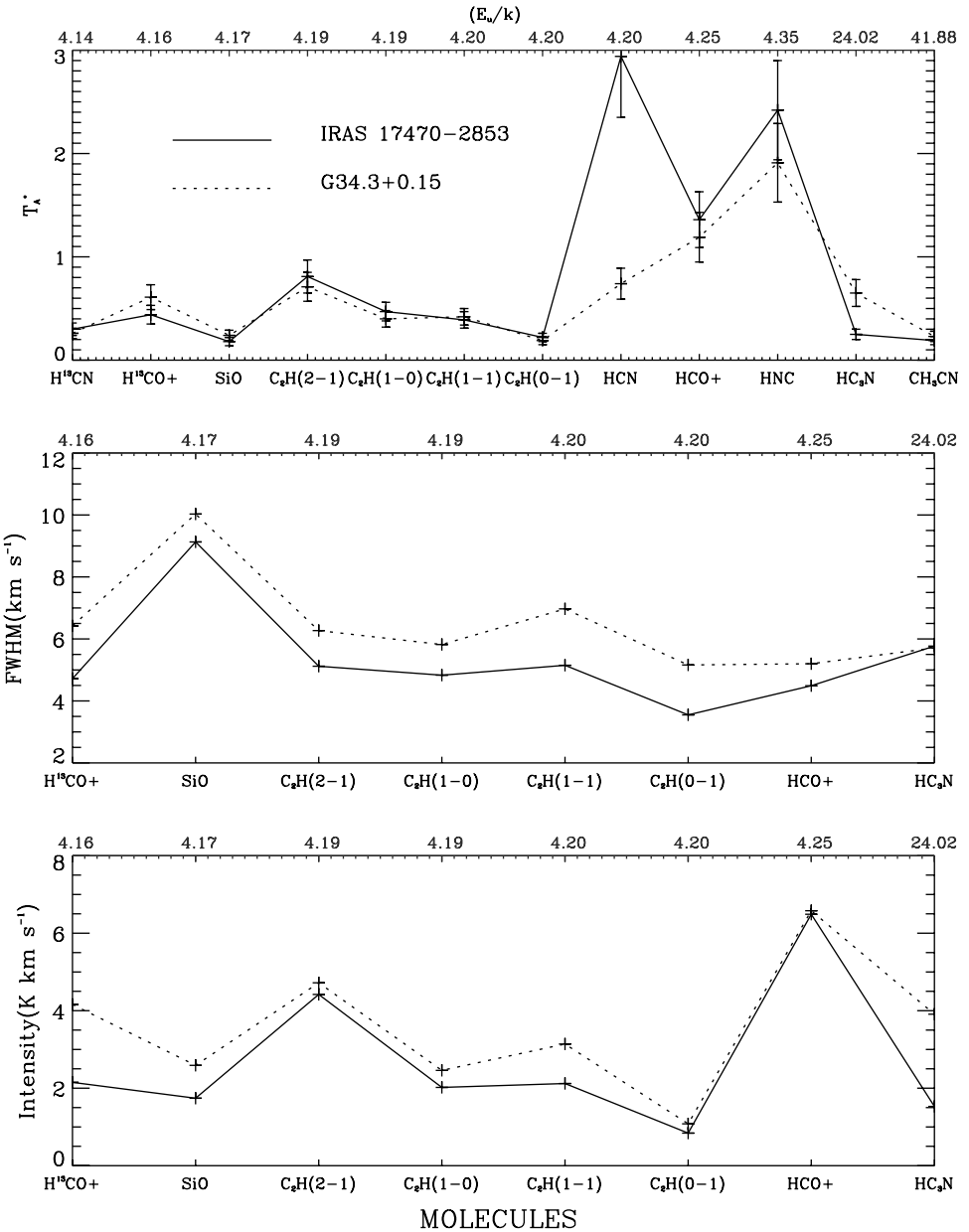

Figure 3 A comparison of T_A^*, line FWHM (in km s^{-1}), and line intensity (in K km s^{-1}) between the different molecules detected by us in IRAS 17470-2853 (solid line) to G34.3+0.15 (dashed line, obtained with the 14 m TRAO telescope by Kim et al. 2000). T_A^* is shown for all lines, whereas the FWHM and line intensity are only shown for lines which are not blended. The upper horizontal axis indicates the energy level of the upper state of each transition. Errors bars show a 20% error determined for absolute calibration.

is not more abundant than HCN. Goldsmith et al. (1981) similarly found HCN to be more abundant in giant molecular clouds with active star formation, such as W51 and Orion. On the other hand, in quiescent dark clouds Irvine & Schloerb (1984) found HNC to be more abundant than HCN, as did Huttemeister et al. (1995) in the extragalactic source Arp 220, a result attributed by the latter authors to emission from a cool, quiescent disk or halo around the source. Thus, the observations of HCN and HNC empirically support IRAS 17470-2853 being warmer than the cold dark clouds.

Finally, we note that HN^{13}C is not detected at 87.09 GHz (Figure 2), whereas it is seen in G34.3+0.15 (Kim et al. 2000). However, this is most likely due to a gap in the spectral coverage at this frequency.

4.2 C_2H and HC_3N

The ratio of abundances, X(C_2H)/X(HC_3N), indirectly tests the chemical formation path, as C_2H and HC_3N are both thought to involve the same precursor, C_2H_2 (Wootten et al. 1980). These authors found the typical ratio to be in the range of 6–10. The most straightforward pathway to the production of C_2H is through ion–electron recombination with $C_2H_2^+$ and $C_2H_3^+$ (Huntress 1977; Herbst, Adams, & Smith 1987). Among the pathways to produce HC_3N is the reaction of C_2H_2 with CN (Herbst &

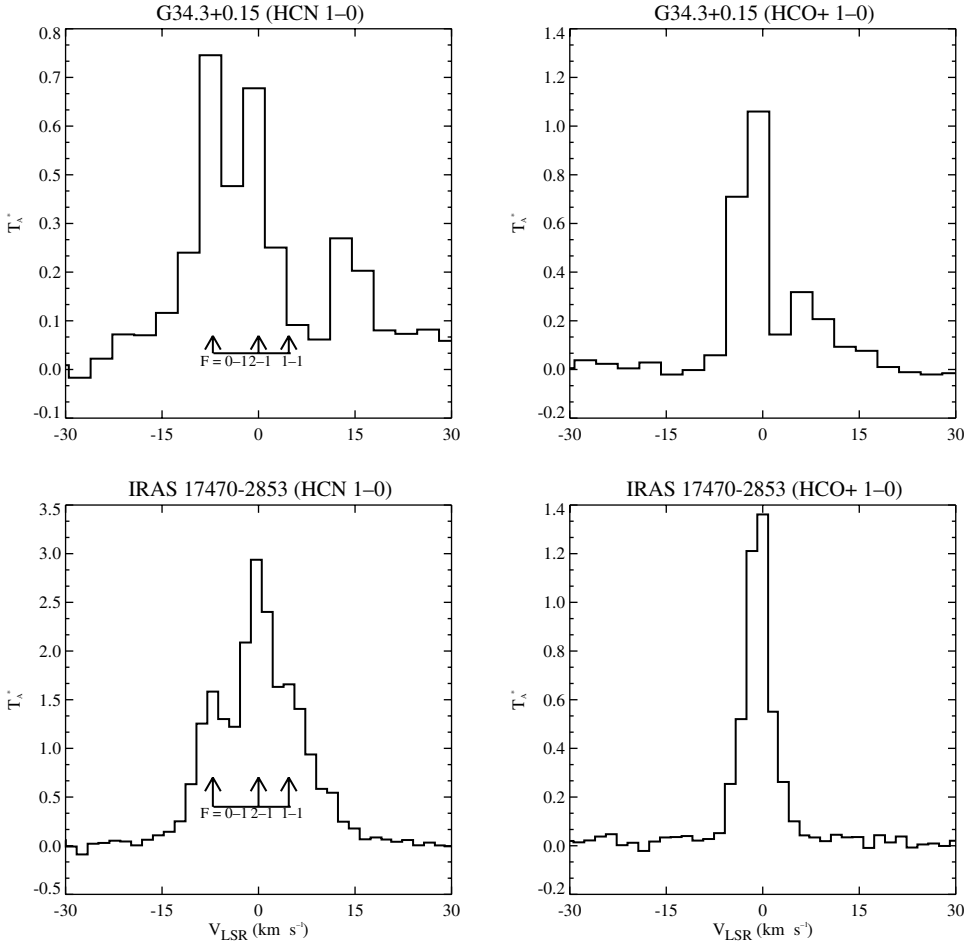

Figure 4 Spectra of HCN (1–0) and HCO^+ (1–0) in G34.3+0.15 (upper panels) and IRAS 17470-2853 (lower panels), as a function of velocity in km s^{-1}. Positive velocity is in the direction of increasing wavelength. Profiles are plotted with respect to the assumed rest velocity for the sources, $V_{\rm LSR} = +58\,km\,s^{-1}$ for G34.3+0.15 and +14 km s^{-1} for IRAS 17470-2853. The three hyperfine components for HCN, $F = 1$–1, 2–1, and 0–1, are marked.

Table 3. Column densities, optical depths, and excitation temperatures derived for observed molecules

Molecule	Column density N_T (cm^{-2})	Optical depth (τ)	Excitation temperature, $T_{\rm ex}$(K)	Notes
HC_3N	$>3.0 \times 10^{13}$		24[a]	From equation (2)
CH_3CN	$>7.7 \times 10^{13}$		28[b]	From equation (3)
HNC	$>2.7 \times 10^{13}$		4[a]	From equation (2)
C_2H	$>5.7 \times 10^{14}$		8[a]	From equation (2)
SiO	$>1.6 \times 10^{12}$		2[a]	From equation (2)
HCN	2.4×10^{14}	3.4	8	Equations (6) to (12)
$H^{13}CN$	7.4×10^{12}	0.1	8	
HCO^+	3.5×10^{13}	2.2	5	Equations (6) to (12)
$H^{13}CO^+$	5.8×10^{12}	0.4	5	

[a] $T_{\rm ex} \sim T_{\rm rot} = E_u/k$.
[b] $T_{\rm ex} \sim T_{\rm rot} = \frac{2}{3} E_u/k$.

Leung 1990; Takano et al. 1998). Unfortunately only lower limits for the abundances of HC_3N and C_2H can be derived from our data set (see Section 5.1), so the abundance ratio cannot be well constrained. However, taking these lower limits (see Table 3) yields a ratio of ∼19 for $X(C_2H)/X(HC_3N)$.

4.3 CH_3CN

This molecule is a symmetric top and all permitted radiative transitions are $\Delta K = 0$. Like other symmetric-top molecules, CH_3CN has been widely used to probe $T_{\rm rot}$, as it has several closely spaced transitions from a wide range of energy levels that can be observed simultaneously, with

collisions only responsible for populating the levels along the K-ladder. Hence, uncertainties arising from calibration errors and antenna gain can be reduced (Loren & Mundy 1984). This molecule forms efficiently by the following reaction route (Millar et al. 1991; Mauersberger et al. 1991):

$$CH_3^+ + HCN \rightarrow CH_3CNH^+$$
$$CH_3CNH^+ + e \rightarrow CH_3CN + H.$$

Since HCN is detected, the possibility of CH_3CN synthesis by the above reaction route may be high. Two transitions from CH_3CN, $J = 5$–4, $K = 2$ and $K = 1$ (the latter blended with the $K = 0$ line), are detected. However, the CH_3CN $J = 5$–4, $K = 4$ and $K = 3$ lines were not seen in IRAS 17470-2853, whereas they were detected in G34.3+0.15. While this is out of expectation based on the relative line ratios in G34.3+0.16 (Kim et al. 2000), the $J = 5$–4, $K = 2$ measurement is close to the detection limit. The missing lines might simply be lost due to poor signal to noise.[2]

4.4 SiO

A line from the molecule SiO was also detected in IRAS 17470-2853. As with G34.3+0.15, the SiO line width is significantly broader than the other lines detected (9 km s^{-1} compared to 4 km s^{-1}). This likely reflects a different origin for the SiO line. Rather than being evaporated off grains in the hot core it is most likely shock-excited, suggesting a mild shock is associated with an embedded source.

4.5 Lines Not Seen

For completeness, we finish this section listing some molecules which were not detected in IRAS 17470-2853, but which might have been expected based on comparison with the hot core in Orion–KL or with Sgr B2 (e.g. Turner 1989). However, we also note that none of these molecules was seen in the 86–92 GHz spectral range in G34.3+0.15, either.

No lines from methanol (CH_3OH) or sulphur dioxide (SO_2) were seen, for instance the usually bright lines emitted by methanol at 86.904 and 88.597 GHz and by sulphur dioxide at 86.641 and 91.550 GHz. The HNCO $4((0,4) - 3(0,3))$ line at 87.925 GHz is particularly strong in Orion–KL and Sgr B2, but is absent in IRAS 17470-2853.

5 Column Densities

When deriving the excitation temperature and column density of a molecule it is preferable to use several transitions arising from a wide range of energy levels. Fitting for the excitation temperature not only reduces errors from using single lines, but also helps to separate the hot core from cooler components in the molecular cloud. The method applied is rotation diagram analysis (see Blake et al. 1987; Macdonald et al. 1996; Kim et al. 2000). This assumes the lines are optically thin and the source is in LTE with a temperature much higher than that of the cosmic background radiation temperature ($T_{\rm bg} = 2.7$ K). When this is so, the equation of radiative transfer can be simplified so that the rotation temperature and total column density can be derived, as follows:

$$N_T = \frac{3k \int T_R^* \, dv}{8\pi^3 \nu \mu^2 S g_I g_K} Q(T_{\rm rot}) \exp\left(\frac{E_u}{kT_{\rm rot}}\right), \quad (1)$$

where ν is the transition frequency, μ the permanent electric dipole moment, k the Boltzmann constant, g_I and g_K are degeneracies, E_u is the upper state energy, S is the line strength, $Q(T_{\rm rot})$ is the partition function for rotational excitation temperature $T_{\rm rot}$, and N_T is the total column density. $\int T_R^* \, dv$ is the integrated line intensity. The reduced nuclear spin weight, g_I, and K-level degeneracy, g_K, of linear molecules are both 1. For CH_3CN, however, $g_K = 1$ for $K = 0$ and $g_K = 2$ for $K \neq 0$, and $g_I = 1/2$ for $K = 3n$ and $g_I = 1/4$ for $K \neq 3n$ (n integer) (Turner 1991).

If several lines are observed it is possible to fit a straight line to a plot of $\ln N_u/g_u = \ln N_T/Q \exp(-E_u/kT)$ against E_u/k, where N_u is the upper state column density, to yield the temperature from the slope and the column density from the intercept. However, with our limited spectral coverage, only a single unblended transition of each molecule has been observed (the 91.9853 and 91.9871 GHz lines of CH_3CN are blended), except for hyperfine transitions of C_2H, HCN and HNC. Since these hyperfine lines cover only a small range of upper state energy levels, we considered them as a single line. It is still possible, though, to derive lower limit values from a single line by assuming that the rotation temperature of linear molecules is $T_{\rm rot} = E_u/k$, and for symmetric or slightly asymmetric tops is $T_{\rm rot} = 2/3\, E_u/k$ (see Macdonald et al. 1996). Then, from equation (1), a lower limit to the column density of linear molecules is given by

$$N_{\rm min} = \frac{3k \int T_R^* \, dv}{8\pi^3 \nu \mu^2 S g_I g_K} Q(T_{\rm rot}) e \quad (2)$$

and for symmetric or slightly asymmetric top molecules by

$$N_{\rm min} = \frac{3k \int T_R^* \, dv}{8\pi^3 \nu \mu^2 S g_I g_K} Q(T_{\rm rot}) e^{3/2}. \quad (3)$$

In the high temperature limit ($hB \ll kT$) diatomic and linear molecules have a partition function

$$Q = \sigma \frac{kT}{hB} \quad (4)$$

where $\sigma = 1$ for HCN, HNC, HCO^+, and SiO, and $\sigma = 3$ for HC_3N to account for the hyperfine splitting (Blake et al. 1987). The partition function for the symmetric molecule CH_3CN has the form

$$Q_{\rm rot} = \frac{2\sigma}{3} [\pi (kT)^3 / h^3 A B^2]^{1/2} \quad (5)$$

[2] In fact, in a deeper spectrum subsequently obtained by us as part of another project, the $K = 3$ line is seen with a similar intensity to the $K = 2$ line.

in the high temperature limit ($hA \ll kT$, $hB \ll kT$), with $\sigma = 3$ to account for hyperfine splitting (Blake et al. 1987).

5.1 HC_3N, CH_3CN, HNC, C_2H, and SiO Lower Limits

Calculating $\int T_R^* \, dv$ as $\int T_A^* \, dv/\eta_{\rm fss}$, we then derive $N_T > 3.0 \times 10^{13}\,{\rm cm}^{-2}$ for the linear molecule HC_3N, and $N_T > 7.7 \times 10^{13}\,{\rm cm}^{-2}$ for the symmetric molecule CH_3CN. For HNC, C_2H, and SiO lower limits of $N_T > 2.7 \times 10^{13}\,{\rm cm}^{-2}$, $N_T > 5.7 \times 10^{14}\,{\rm cm}^{-2}$, and $N_T > 1.6 \times 10^{12}\,{\rm cm}^{-2}$ are derived, respectively. These limits are listed in Table 3.

We can compare the limits for HC_3N and CH_3CN with column densities obtained in other surveys. An analysis of data from the NRAO 12 m telescope for Sgr B2 and Orion–KL (Turner 1991) obtained $N_T = 3.1 \times 10^{14}\,{\rm cm}^{-2}$ for HC_3N and $N_T = 1.0 \times 10^{14}\,{\rm cm}^{-2}$ for CH_3CN in Sgr B2, and $N_T = 4.6 \times 10^{13}\,{\rm cm}^{-2}$ for HC_3N and $N_T = 5.6 \times 10^{13}\,{\rm cm}^{-2}$ for CH_3CN in Orion–KL. In G34.3+0.15, Kim et al. (2000) obtained $N_T = 1.1 \times 10^{14}$ cm^{-2} for HC_3N and $N_T = 1.7 \times 10^{14}$ for CH_3CN. Olmi, Cesaroni, & Walmsley (1993) observed CH_3CN towards 11 ultracompact HII regions, finding column densities in the range 2–12 $\times 10^{13}\,{\rm cm}^{-2}$ and rotational temperatures from 8 to 23 K, applying the rotational temperature method.

5.2 HCN and HCO^+

For HCN and HCO^+ the isotopes $H^{13}CN$ and $H^{13}CO^+$ have also been observed. Assuming the isotopes are optically thin, the main lines are optically thick, and that the levels are in LTE, we can determine the column density, optical depth, and excitation temperature for these molecules as follows:

The equation of radiative transfer is

$$T_R^* = [J(T_{\rm ex}) - J(T_{\rm bg})](1 - e^{-\tau}) \tag{6}$$

with

$$J(T) = T_0 \left[e^{h\nu/kT} - 1 \right]^{-1}, \tag{7}$$

where $T_0 = h\nu/k$. For an optically thick line ($\tau \gg 1$)

$$T_{\rm ex} = \frac{T_0}{\ln\left(\frac{T_0}{T_R^* + J(T_{\rm bg})} + 1\right)}. \tag{8}$$

On the other hand, if the excitation temperature, $T_{\rm ex}$, is known, then the optical depth is given by

$$\tau = -\ln\left(1 - \frac{T_R^*}{J(T_{\rm ex}) - J(T_{\rm bg})}\right). \tag{9}$$

The optical depth, τ, is related to the column density and excitation temperature by

$$\tau = \frac{8\pi^3 \mu^2 N}{3h\Delta v Q}\left[1 - e^{-h\nu/kT_{\rm ex}}\right]. \tag{10}$$

From equation (10) we can also relate the optical depth of the main line and the isotope by

$$\frac{\tau_{\rm main}}{\tau_{\rm isotope}} \sim \frac{N_{\rm main}}{N_{\rm isotope}} = {\rm X}, \tag{11}$$

where X is the abundance ratio of the main species to its isotope. From equation (6), the ratio of the measured intensities, R, is given by

$$R = \frac{T_{R,{\rm main}}^*}{T_{R,{\rm isotope}}^*} \sim \frac{1 - e^{-\tau_{\rm main}}}{1 - e^{-\tau_{\rm isotope}}}, \tag{12}$$

which lets us calculate $\tau_{\rm main}$. Finally, applying equation (11), and assuming the isotope is optically thin, we obtain

$$R = \frac{1 - e^{-\tau_{\rm main}}}{\tau_{\rm main}}{\rm X}. \tag{13}$$

Thus, if we assume the main line is optically thick we can derive $T_{\rm ex}$ from the measured T_R^* (equation (8)). By assuming the isotope has the same excitation temperature as the main line we derive $\tau_{\rm isotope}$ (equation (9)). Equation (10) then determines the column density of the isotope, equation (12) the optical depth of the main line, and equation (11) its column density.

For HCN we obtain $T_{\rm ex} \sim 8$ K and for $H^{13}CN$ $\tau \sim 0.1$ and $N_T \sim 7.4 \times 10^{12}\,{\rm cm}^{-2}$. This then determines for HCN that $\tau \sim 3.4$ and $N_T \sim 2.4 \times 10^{14}\,{\rm cm}^{-2}$.

For HCO^+ we obtain $T_{\rm ex} \sim 5$ K and for $H^{13}CO^+$ $\tau \sim 0.4$ and $N_T \sim 5.8 \times 10^{12}\,{\rm cm}^{-2}$. This then determines for HCO^+ that $\tau \sim 2.2$ and $N_T \sim 3.5 \times 10^{13}\,{\rm cm}^{-2}$. These results are summarised in Table 3.

6 Summary

We report the results of the first molecular line survey carried out with the Mopra telescope, towards the massive young stellar source IRAS 17470-2853. Twenty-one molecular transitions from 9 species were detected. We have compared the results to a similar survey for the ultracompact HII region G34.3+0.15.

On the whole, the chemical compositions of IRAS 17470-2853 and G34.3+0.15 are similar. However there are some differences, as might be expected if the sources are at different evolutionary stages. We have found that IRAS 17470-2853 has narrower line widths and weaker antenna temperatures. Self-absorption is not seen in HCO^+ and the ratio of HNC/HCN is significantly lower. There is also a minor difference in the number of lines of CH_3CN that are detected.

The relatively large line width of SiO ($v = 0$, $J =$ 2–1) compared to other molecules seen suggests that shock chemistry is occurring, possibly as a result of winds originating from an embedded source.

The isotopic molecules $H^{13}CN$ and $H^{13}CO^+$ are seen, as are C_2H and HC_3N. These molecules are seen in G34.3+0.15 too. However, as in G34.3+0.15, but unlike in the Orion hot core, lines from the molecules CH_3OH, SO_2 and HNCO are not seen from 86–92 GHz.

The richness of the spectrum in the relatively small bandpass surveyed suggests that IRAS 17470-2853 will be a fruitful source for further observation, like G34.3+0.15. More comprehensive line surveys of a variety of hot molecular cores, to compare and contrast the molecular

lines present and their physical characteristics, will provide a tool to study the chemistry of star forming clouds, and the evolutionary stages which they go through as a star is formed. Our data suggest that IRAS 14070-2853 is in a slightly earlier evolutionary stage than G34.3+0.15.

Acknowledgements

This work would not have been possible without the support of the Australia–Korea Foundation. A number of other people have also made significant contributions to the observational program with the Mopra telescope to whom we are grateful: Tamara Davis, Jung-Kyu Lee, Michael Murphy, Jill Rathborne, Angie Schultz, and John Storey from the University of New South Wales, and Graeme Carrad, Michael Kesteven, and Ray Norris from the Australia Telescope National Facility. We also had useful discussions with Andrew Walsh. Finally, we wish to thank the anonymous referees, whose comments and criticisms have led to a greatly improved paper. The Mopra telescope is operated through a collaborative arrangement between the University of New South Wales and the CSIRO.

References

Baudry, A., Combes, M., Perault, M., & Dickman, R. 1980, A&A, 85, 244
Blake, G. A., Sutton, E. C., Masson, C. R., & Phillips, T. G. 1986, ApJS, 60, 357
Blake, G. A., Sutton, E. C., Masson, C. R., & Phillips, T. G. 1987, ApJ, 315, 621
Blake, G. A., Mundy, L. G., Carlstrom, J. E., Padin, S., Scott, S. L., Scoville, N. Z., & Woody, D. P. 1996, ApJ, 472, 49
Brown, R. D., Burden, F. R., & Cuno, A. 1989, ApJ, 347, 855
Cernicharo, J., Castets, A., Duvert, G., & Guilloteau, S. 1984, A&A, 139, L13
Charnley, S. B., Kress, M. E., Tielens, A. G. G. M., & Millar, T. J. 1995, ApJ, 448, 232
Cummins, S. E., Linke, R. A., & Thaddeus, P. 1986, APJ, 60, 819
Forster, J. R., & Caswell, J. L. 1999, A&AS, 137, 43
Garwood, R. W., & McMullin, J. P. 1999, AIPS++ NOTE 225– Using Dish: The AIPS++ Single Dish Analysis Environment, http://aips2.nrao.edu/docs/aips++.html
Goldsmith, F. P., Langer, W. D., Ellder, J., Irvine, W., & Kollberg, E. 1981, ApJ, 249, 524
Henkel, C., Mauersberger, R., Wilson, T. L., Snyder, L. E., Menten, K., & Wouterloot, J. G. A. 1987, A&A, 182, 299
Herbst, E., Adams, N. G., & Smith, D. 1987, ApJ, 312, 351
Herbst, E., & Leung, C. M. 1990, A&A, 233, 177
Huntress, W. T. 1977, ApJS, 33, 495
Huttemeister, S., Henkel, C., Mauersberger, R., Brouillet, N., Wiklind, T., & Millar, T. J. 1995, A&A, 295, 571
Irvine, W. I., & Schloerb, F. P. 1984, ApJ, 282, 516
Jewell, P. R., Hollis, J. M., Lovas, F. J., & Snyder, L. E. 1989, ApJS, 70, 833
Johansson, L. E. B., et al. 1984, A&A, 130, 227
Kim, H.-D., Cho, S.-H., Chung, H.-S., Kim, H.-R., Roh, D.-G., Kim, H.-G., Minh, Y. C., & Minn, Y.-K. 2000, ApJS, 131, 483
Loren, R. B., & Mundy, L. G. 1984, ApJ, 286, 232
Lovas, F. J. 1992, JPCRD, 21, 181
Macdonald, G. H., Gibb, A. G., Harbing, R. J., & Millar, T. J. 1996, A&AS, 119, 333
Mauersberger, R., Henkel, C., Walmsley, C. M., Sage, L. J., & Wiklind, T. 1991, A&A, 247, 307
Millar, T. J., Herbst, E., & Charnley, S. B. 1991, A&A, 369, 147
Millar, T. J., Macdonald, G. H., & Gibb, A. G. 1997, A&A, 325, 1163
Olmi, L., Cesaroni, R., & Walmsley, C. M. 1993, A&A, 276, 489
Schilke, P., Walmsley, C. M., Pineau des Forets, G., Roueff, E., Flower, D. R., & Guilloteau, G. 1992, A&A, 256, 595
Schilke, P., Groesbeck, T. D., Blake, G. A., & Phillips, T. G. 1997, ApJS, 108, 301
Sutton, E. C., Jaminet, P. A., Danchi, W. C., & Blake, G. A. 1991, ApJS, 77, 255
Takano, S., et al. 1998, A&A, 329, 1156
Turner, B. E. 1989, ApJS, 70, 539
Turner, B. E. 1991, ApJS, 76, 617
Ulich, B. L., & Haas, R. W. 1976, ApJS, 30, 247
Walmsley, C. M., Hersen, W., Henkel, C., Mauersberger, R., & Wilson, T. L. 1987, A&A, 172, 311
Walsh, A. J., Hyland, A. R., Robinson, G., & Burton, M. G. 1997, A&A, 291, 261
Walsh, A. J., Burton, M. G., Hyland, A. R., & Robinson, G. 1998, A&A, 301, 640
Walsh, A. J., Macdonald, G. H., Alvey, N. P. S., Burton, M. G., & Lee, J.-K. 2002, A&A, submitted
Wootten, A., Evans II, N. J., Snell, R., & Vanden Bout, P. 1978, ApJ, 225, L143
Wootten, A., Bozyan, E. P., & Garrett, D. B. 1980, ApJ, 239, 844
Ziurys, L. M., & McGonagle, D. 1993, ApJS, 89, 155